Short article

Developmental Cell

ERK synchronizes embryonic cleavages in *Drosophila*

Graphical abstract

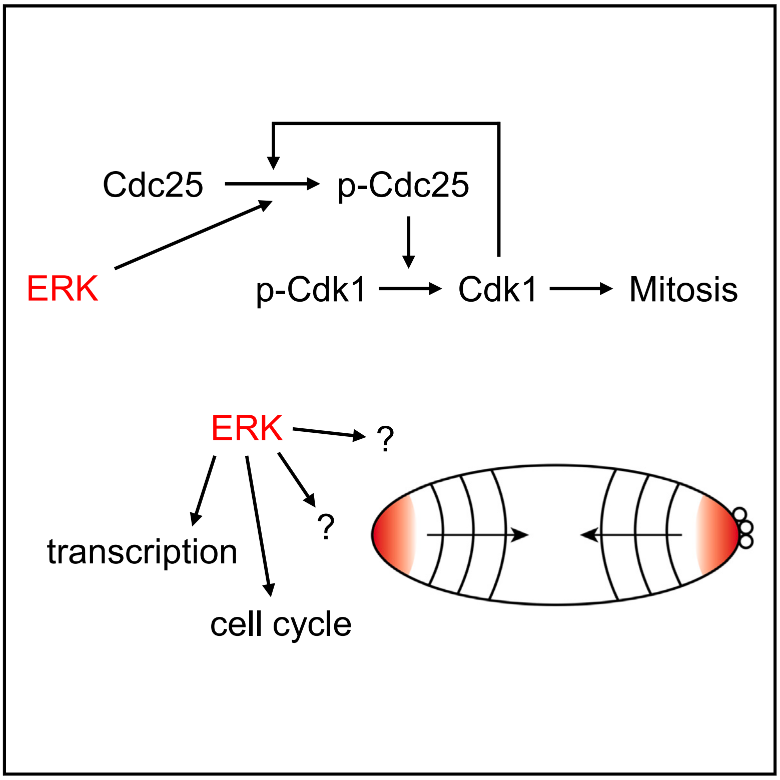

Highlights

- ERK signaling investigated using optogenetics and phosphoproteomics
- ERK controls the speed and synchrony of embryonic cleavages
- Localized ERK signaling acts as a pacemaker for mitotic entry

Authors

Liu Yang, Audrey Zhu,
Javed M. Aman, ..., Mona Singh,
Martin Wühr, Stanislav Y. Shvartsman

Correspondence

wuhr@princeton.edu (M.W.),
stas@princeton.edu (S.Y.S.)

In brief

Yang et al. report that, in addition to its well-known role in the transcriptional patterning of the *Drosophila* embryo, the first wave of ERK signaling also synchronizes embryonic cleavage divisions.

Yang et al., 2024, Developmental Cell *59*, 1–11
December 2, 2024 © 2024 Published by Elsevier Inc.
https://doi.org/10.1016/j.devcel.2024.08.004

CellPress

Please cite this article in press as: Yang et al., ERK synchronizes embryonic cleavages in *Drosophila*, Developmental Cell (2024), https://doi.org/10.1016/j.devcel.2024.08.004

Developmental Cell

CellPress

Short article

ERK synchronizes embryonic cleavages in *Drosophila*

Liu Yang,[1,8] Audrey Zhu,[1,2,8] Javed M. Aman,[1,3] David Denberg,[1,4] Marcus D. Kilwein,[5] Robert A. Marmion,[1] Alex N. T. Johnson,[1,2,5] Alexey Veraksa,[6] Mona Singh,[1,3] Martin Wühr,[1,2,5,*] and Stanislav Y. Shvartsman[1,4,5,7,9,*]

[1]Lewis Sigler Institute for Integrative Genomics, Princeton University, Princeton, NJ 08544, USA
[2]Department of Chemical & Biological Engineering, Princeton University, Princeton, NJ 08544, USA
[3]Department of Computer Science, Princeton University, Princeton, NJ 08544, USA
[4]Program in Quantitative and Computational Biology, Princeton University, Princeton, NJ 08544, USA
[5]Department of Molecular Biology, Princeton University, Princeton, NJ 08544, USA
[6]Department of Biology, University of Massachusetts Boston, Boston, MA 02125, USA
[7]Flatiron Institute, New York, NY 10010, USA
[8]These authors contributed equally
[9]Lead contact
*Correspondence: wuhr@princeton.edu (M.W.), stas@princeton.edu (S.Y.S.)
https://doi.org/10.1016/j.devcel.2024.08.004

SUMMARY

Extracellular-signal-regulated kinase (ERK) signaling controls development and homeostasis and is genetically deregulated in human diseases, including neurocognitive disorders and cancers. Although the list of ERK functions is vast and steadily growing, the full spectrum of processes controlled by any specific ERK activation event remains unknown. Here, we show how ERK functions can be systematically identified using targeted perturbations and global readouts of ERK activation. Our experimental model is the *Drosophila* embryo, where ERK signaling at the embryonic poles has thus far only been associated with the transcriptional patterning of the future larva. Through a combination of live imaging and phosphoproteomics, we demonstrated that ERK activation at the poles is also critical for maintaining the speed and synchrony of embryonic cleavages. The presented approach to interrogating phosphorylation networks identifies a hidden function of a well-studied signaling event and sets the stage for similar studies in other organisms.

INTRODUCTION

A genetic approach to developmental signaling most commonly starts with a morphological defect caused by the disruption of one component. An epistasis analysis then follows to construct a circuit by which a signaling event is causally linked to a developmental outcome. This powerful approach has led to the discovery of most ligands, receptors, and intracellular proteins that control tissue patterning, growth, and morphogenesis.[1–3] This strategy, however, relies on examining the effects of genetic perturbations several steps after a signaling event has occurred. Consequently, the circuits emerging from genetic studies may lack key components, especially those that control ubiquitously used cellular processes. Here, we show how the genetics-based circuitry can be systematically augmented using global analysis of short-term biochemical effects of optogenetic perturbations. We illustrate this approach by identifying a hitherto hidden function for a signaling event in the *Drosophila* embryo.[4,5]

Most animals start their development with a series of rapid mitotic divisions, during which the large egg is progressively partitioned into smaller and smaller cells.[6] These cleavage divisions ensure efficient generation of a large number of zygotic genomes that are placed in cells with normalized ratios of nuclear and cytoplasmic volumes and can proceed to realize their species-specific developmental potential.[7] Some of the fastest embryonic cleavages have been observed in embryos of *Drosophila melanogaster*, where 13 successive division cycles are completed within just 2 h of fertilization, before the major wave of zygotic gene activation and formation of the cell membranes. The first seven cleavages are accompanied by self-organized cytoplasmic flows that spread the nuclei along the anteroposterior axis of the egg.[8,9] After the next two cycles, most of the nuclei are found under the common plasma membrane, where they divide four more times, generating a blastoderm with ~6,000 uniformly distributed nuclei.

The first nine cleavages are fast and synchronous, with minimal differences in the timing of mitotic entry across the embryo. The last four divisions, however, are characterized by progressive slowing down and loss of synchrony, with mitotic entry starting at the embryonic poles and spreading toward the middle of the embryo.[10] Although the deceleration of the cleavages has been conclusively linked to the activation of the DNA damage checkpoint pathway,[9,11] the cause of advanced mitotic entry at the poles remained unknown, even though the effect was already noted in early studies of embryonic cleavages.[6,12–14] Below, we propose a plausible model for this effect and test it using genetic, imaging, and phosphoproteomic experiments.

RESULTS

Terminal ERK signaling is required for synchrony of late cleavage divisions

Because mitotic entry is universally controlled by the kinase activity of the CyclinB/Cyclin-dependent kinase 1 (CDK1) complex (henceforth, just CDK),[15] the cause for advanced mitotic entry at the poles can be sought in the additional positive input into CDK activation at the embryo's terminal regions. When combined with the self-amplifying nature of CDK activation and diffusion in the syncytium, such region-specific positive control of CDK could explain the observed initiation of mitotic waves at the termini and subsequent propagation through the blastoderm[16] (Figure 1A). Studies in Xenopus embryos and mammalian cells have established that CDK activity could be positively regulated by the highly conserved extracellular-signal-regulated kinase (ERK).[17] ERK and Cdk1 phosphorylates Cdc25 threonine 138 in *Xenopus* (serine 76 in flies and threonine 130 in humans), thereby activating the Cdc25 phosphatase, which is, in turn, essential for reversing the inhibitory phosphorylations of the highly conserved threonine and tyrosine residues in CDK (Figure 1B).

Interestingly, ERK is activated at the poles of the fly embryo at the time of the last four syncytial cleavages, suggesting that it might be involved in the initiation of mitotic waves at the poles (Figure 1C). ERK activation at the poles is caused by the spatially restricted signaling through Torso, a uniformly expressed receptor tyrosine kinase that is stimulated by its locally processed ligand trunk.[18] Thus far, Torso-dependent ERK signaling has been linked only to the transcriptional patterning of the blastoderm. Based on the spatiotemporal correlation between the advanced mitotic entry and ERK activation at the poles, we hypothesized that terminal ERK signaling has an additional role in regulating the embryonic cleavages.

As a first step in testing this hypothesis, we analyzed the effects of disrupting ERK activation throughout the embryo. A maternal Gal4 driver was used to express an RNAi construct directed against mitogen-activated protein kinase (MEK), a kinase that induces the enzymatic activity of ERK by phosphorylating a tyrosine and threonine residue within its activation loop.[19] The efficiency of this perturbation is demonstrated by complete loss of dually phosphorylated ERK (dpERK) at the poles, strong embryonic lethality, and complete loss of the non-segmented terminal regions of the larva, which are known to depend on terminal ERK signaling[5] (Figures 1D and S1A). In addition to examining fixed embryos and larval cuticles, we used live imaging of embryos with fluorescently tagged S-phase Cyclin, Cyclin E (CycE-sfGFP[20]) to examine the potential effects of disrupted ERK activation on the embryonic cleavages.

Uniform disruption of ERK activation in the early embryo caused significant lengthening of the last two cleavages, with the median durations of each of the last two cycles increasing by ~4 min (Figure 1E). This effect was observed with two independent MEK RNAi constructs (Figure 1E) and is readily visible (Figures S1B and S1C; Video S1), with a single propagating wave instead of the normal pattern with two fast waves originating from the poles (Figure S1D). Thus, in addition to the localized effect at the poles, where ERK signaling patterns the non-segmented terminal regions of the future larva,[5] ERK signaling also controls the spatiotemporal pattern of mitotic cleavages. Consistent with this conclusion, we found that the normal pattern of inward-propagating mitotic entry was disrupted in embryos that lack trunk, which is essential for ERK activation at the poles.[21] Propagating waves were still observed, but could sometimes initiate away from the poles and lacked the one-dimensional character seen in wild-type (WT) embryos (Figure S1D).

Localized ERK activation can trigger mitotic entry

The above results suggest that Torso-dependent ERK activation acts as a pacemaker of the later syncytial cleavages, when the mitotic oscillator is slowed down by the activation of the DNA damage checkpoint pathway.[6,12,13] To test whether localized ERK signaling is not only necessary but also sufficient for triggering mitotic entry in cleavage-stage embryos, we used the optoSos system for rapid ERK activation independently of extracellular signals.[22] This approach relies on the blue-light-dependent membrane recruitment of the catalytically active form of Sos, a guanine nucleotide exchange factor that triggers a cascade leading to ERK activation (Figure 2A, left). Recent studies have demonstrated that such optogenetic activation of ERK can fully substitute the effects of trunk-dependent Torso signaling.[23] We therefore tested whether an additional light-induced center of ERK activation can act as an origin of mitotic entry (Figure 2A, middle). In these experiments, the components of the optoSos system were introduced into embryos expressing histone-mIFP, which illuminates chromatin morphology (Figure 2A, right).

We found that a spatial pulse of ERK activation positioned in the middle of the anteroposterior axis serves as a robust source of mitotic entry, generating a pattern that differs from what is observed in normal embryos (Figures 2B and 2C; Video S2). Optogenetic ERK activation could induce mitotic entry only in the last two cleavages. Longer oscillation periods create more potential for mitotic asynchrony across the embryo. Thus, we suggest that ERK is needed for orchestrating mitotic entry during the later cycles, when free running mitotic oscillators are slowed down by the checkpoint pathway.[11,24]

What can be the mechanism connecting active ERK to mitotic entry? One possible connection, already mentioned above, could rely on the ERK-dependent control of CDK1 via phosphorylation of Cdc25. This would suggest that *Drosophila* Cdc25 proteins are phosphorylated by ERK, which is certainly possible given that two Cdc25 proteins are expressed and functional at this stage of development.[25–27] A more complex mechanism is also possible because ERK can phosphorylate other proteins involved in the processes leading to and accompanying mitosis, such as spindle formation and nuclear envelope breakdown.[28,29]

ERK activation triggers rapid phosphoproteomic response

As an unbiased approach for probing such connections, we analyzed global changes of protein phosphorylation triggered by acute ERK activation. First, we found that a 10-min pulse of

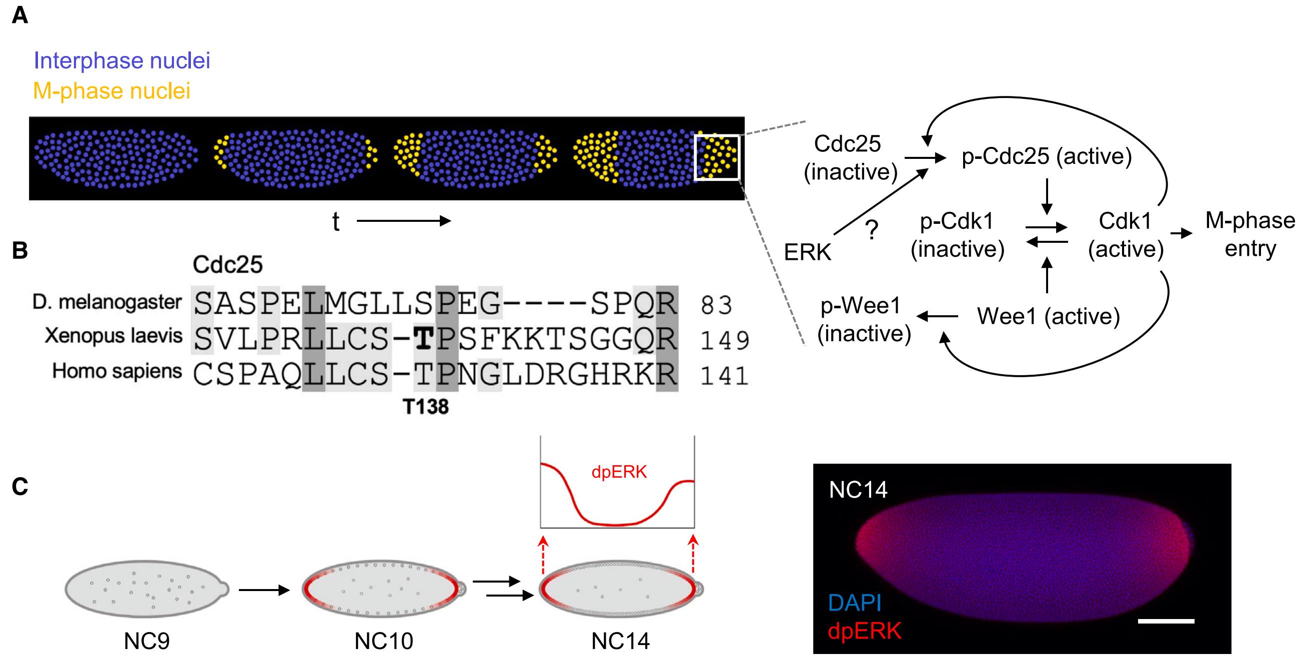

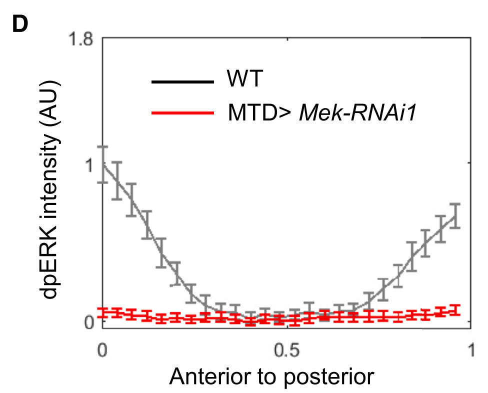

E

Mean Cell Cycle Time (min)

	Control	*Mek-RNAi1*	*Mek-RNAi2*	*Torso-RNAi*
NC10	11±0.5	11.2±0.5	11.4±0.5	11.4±1.0
NC11	12±0.5	13±0.8*	13.7±1.2	12.7±0.9
NC12	14.6±1	17.3±1***	17.7±2**	15.7±1.5
NC13	22.6±1.5	26.8±2.2**	28.3±4.9*	25.7±2.0**

Figure 1. Terminal ERK signaling is required for synchrony of late cleavage divisions

(A) Schematic of initiation of mitotic waves at the termini (left to right). Interphase and mitotic-phase nuclei are labeled as blue and yellow, respectively.

(B) *D. melanogaster* Cdc25 SP site with the best alignment to a known and functionally relevant ERK target site from *X. laevis* (T138, in bold).

(C) Left, schematic of early fly embryo development showing the timing and location of the Torso-dependent ERK signaling (red). Right, representative image of a wild-type NC14 embryo. Scale bars, 100 μm.

(D) dpERK profiles from immunofluorescence (IF) images from the wild-type (n = 12) and *Mek-RNAi1* (n = 20) embryos. Error bars denote standard error of the mean.

(E) Mean cell-cycle times from *mCherry-RNAi* (control, n = 7), *Mek-RNAi1* (n = 5), *Mek-RNAi2* (n = 6), and *Torso-RNAi* (n = 6) embryos.

Data are represented as mean ± SEM. p values were obtained by Student's t test (two-sided, homoscedastic): ***$p < 0.001$, **$p < 0.01$, *$p < 0.05$, NS: $p > 0.05$. See also Figure S1 and Video S1.

optoSos stimulation establishes a signaling state where the entire embryo is exposed to the level of ERK activation that is normally restricted to the poles (Figures 3A, S2A, and S2B). Next, we used quantitative phosphoproteomics to compare abundances of phosphopeptides in 10-min-light-stimulated and control embryos (Figures 3B and 3C; Table S1). Consistent with the large increase of the dpERK signal detected by antibody staining of fixed embryos, our phosphoproteomic data revealed a large increase in the abundance of phosphopeptides from the ERK activation loop (Figure 3D). We also detected an increased abundance of phosphopeptides from capicua (Cic), an ERK substrate that is essential for patterning effects of Torso[32–34](Figure 3D).

A large group of proteins responds similarly to ERK and Cic. One of these proteins was Cdc25 (String [Stg]), which showed a clear increase in the abundance of the phosphosite S76/S80, corresponding to T138 in *Xenopus* Cdc25, that was identified by studies of the ERK-dependent control of its phosphatase activity[17] (Figures 3C and 3D). Consistent with these changes in the phosphorylation status of Cdc25, we detected a significant decrease in the phosphorylation of the inhibitory phosphosites of CDK1 (T14 and Y15) (Figure 3C). Because these sites are

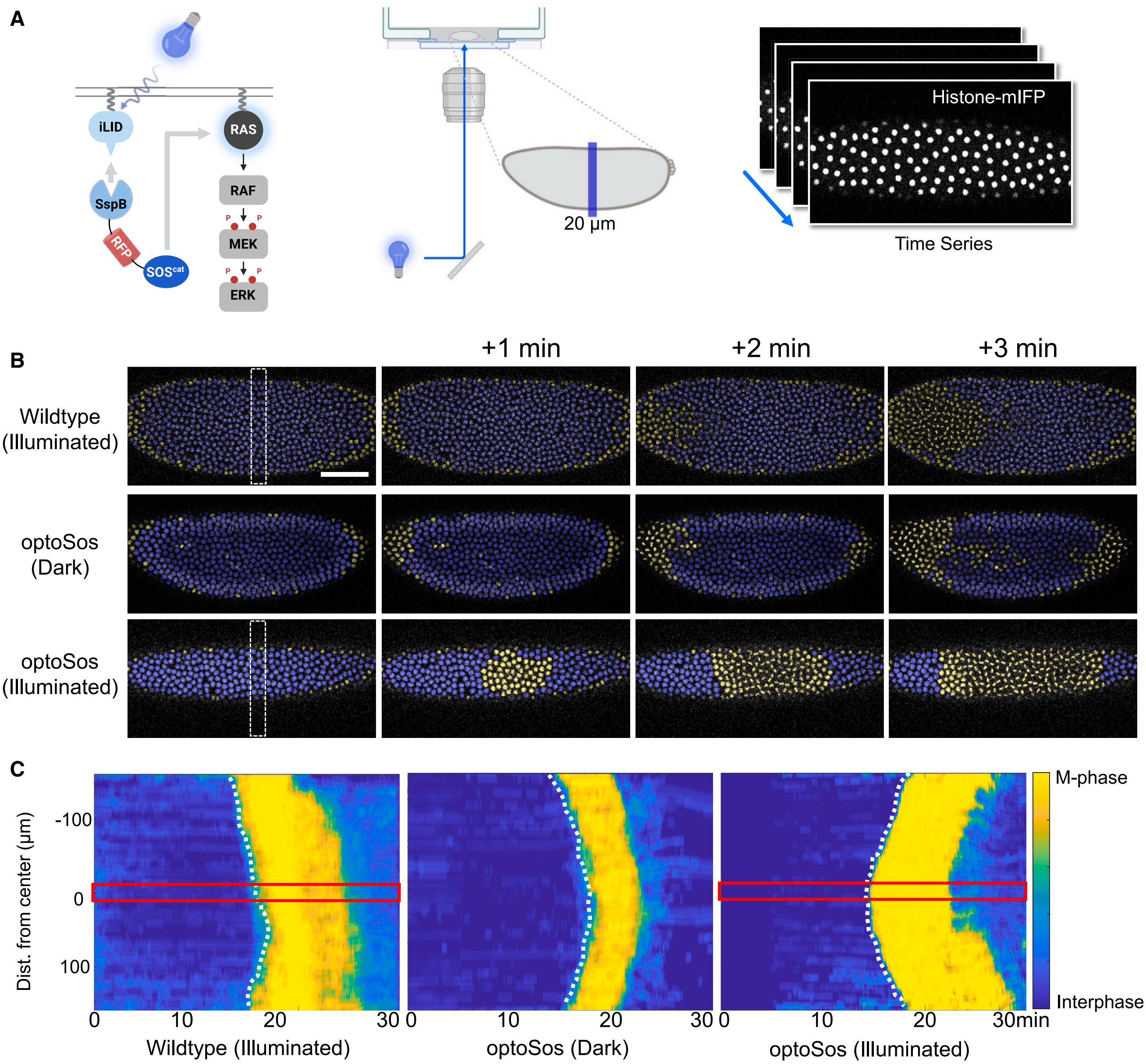

Figure 2. Localized ERK activation can trigger mitotic entry in the syncytial embryo

(A) Schematic of the optogenetic system for ERK activation. The embryo was illuminated from NC11 in a 20-µm stripe generated by a digital mirror device. The illuminated region is marked by blue from the top view of the embryo. Right: z stacks were obtained every 6 s and interphase and M-phase nuclei were marked by histone-mIFP.

(B) Still images from time-lapse imaging of wild-type or optoSos embryos. Interphase and M-phase nuclei were marked by yellow and blue, respectively. Scale bar, 50 µm. The dotted box indicates the illuminated region.

(C) A kymograph of the nuclear phase along the anterior-posterior axis of embryos from (B). Dotted lines indicate the mitotic entry front. The red box shows the width (20 µm) of the illuminated region.

See also Video S2.

phosphorylated by the Wee1 kinase and dephosphorylated by Cdc25, the net decrease of their abundance could come from the increased phosphatase activity of Cdc25 and from the decreased kinase activity of Wee1, which is known to be inhibited when phosphorylated by CDK1. Consistent with this, we found a significant increase in the inhibitory phosphorylation of Wee1 (Figures 3C and 3D).[35]

Thus, the Cdc25/Wee1/CDK1 circuit, which mediates irreversible mitotic entry in a wide range of cell types, can be positively regulated by ERK signaling in the early embryo. This conclusion is further supported by the phosphoproteomic response of embryos that received an even shorter, 3-min pulse of optoSos activation. Analysis of this response showed a striking increase in Cdc25 phosphorylation on the same site discussed previously,

Please cite this article in press as: Yang et al., ERK synchronizes embryonic cleavages in *Drosophila*, Developmental Cell (2024), https://doi.org/10.1016/j.devcel.2024.08.004

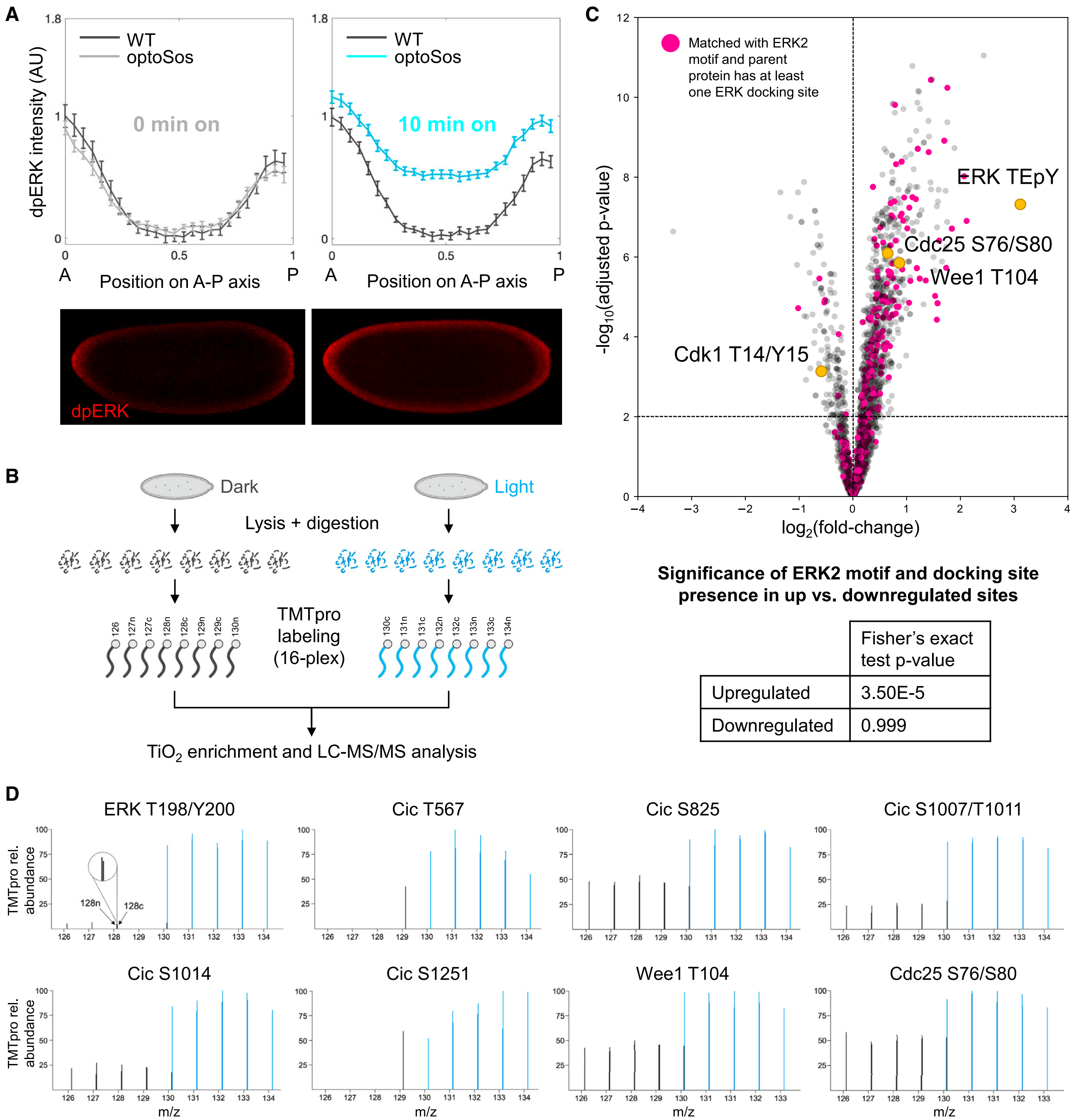

	Fisher's exact test p-value
Upregulated	3.50E-5
Downregulated	0.999

Figure 3. Optogenetic ERK activation triggers rapid phosphoproteomic response

(A) dpERK profiles from the wild-type embryos (n = 15) and optoSos-expressing embryos exposed to either no blue light (n = 11, left) or 10 min of blue light (n = 18, right). Error bars denote standard error of the mean. Representative IF images of optoSos embryos illuminated with 0 or 10 min blue light are shown below their respective profiles.

(B) Sample preparation workflow for phosphoproteomics.

(C) Top: volcano plot depicting phosphosites changing in response to 10 min of optoSos activation. Sites were scored for matches to the ERK2 phosphorylation site.[30] Those that matched with ERK2 and whose parent protein had at least one ERK docking site[31] are highlighted in magenta. Sites on ERK, Cdc25, Wee1, and Cdk1 are highlighted in yellow. p values are Benjamini-Hochberg adjusted. Bottom: a one-sided Fisher's exact test was used to evaluate the significance of the proportion of "motif + docking site" sites in upregulated and downregulated quadrants.

(D) MS3 spectra for the dpERK peptide, five CIC phosphopeptides, and peptides from Cdc25 and Wee1. The spectra show the relative abundance changes of peptides via the TMTpro reporter ions.

See also Figures S2 and S3 and Table S1.

Please cite this article in press as: Yang et al., ERK synchronizes embryonic cleavages in *Drosophila*, Developmental Cell (2024), https://doi.org/10.1016/j.devcel.2024.08.004

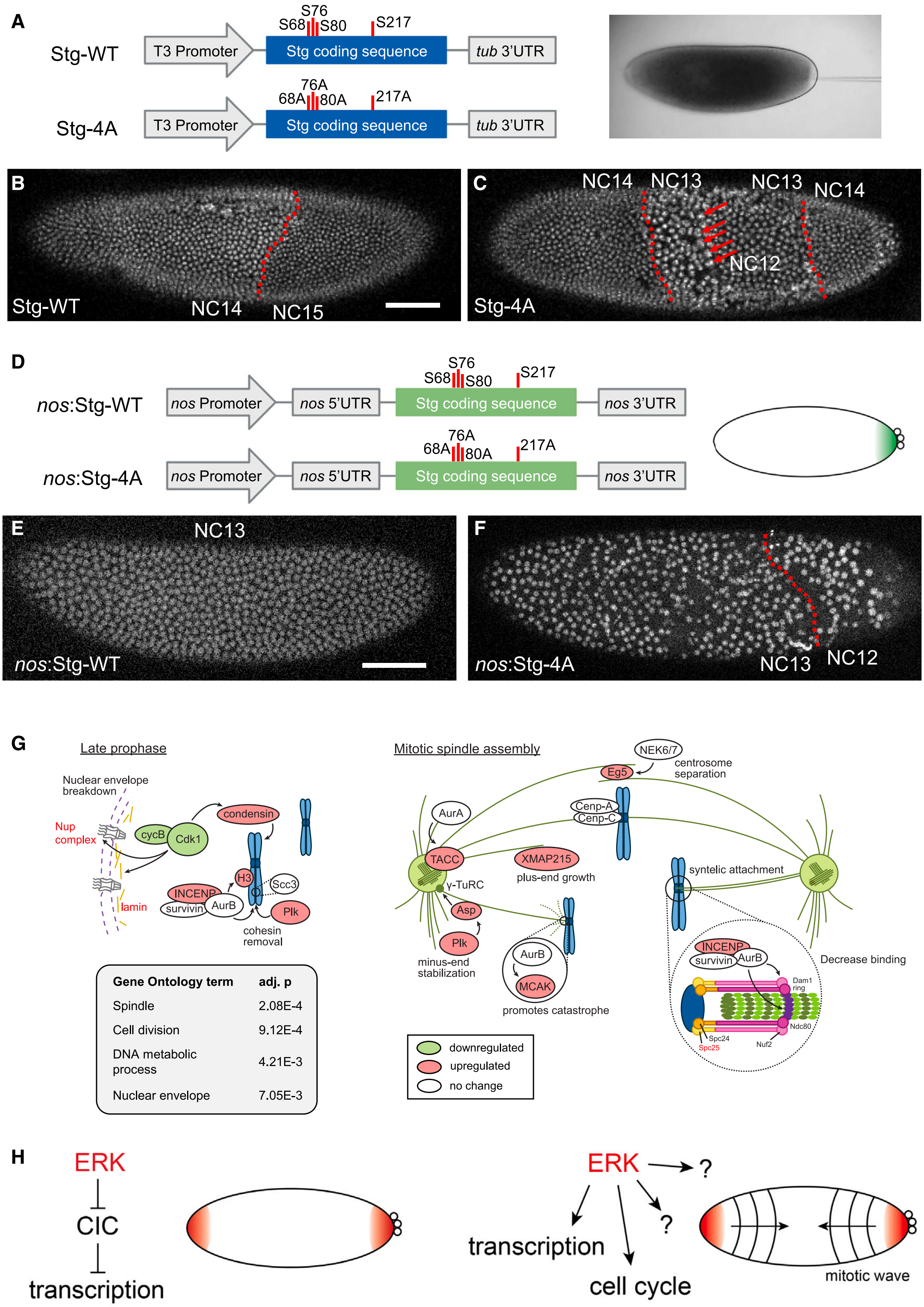

(legend on next page)

as well as downregulation of CDK1's inhibitory sites (Figure S2C; Table S1). Because the early fly embryo is a syncytium where nearby regions are coupled by diffusion and other transport mechanisms, the ERK-dependent induction of the state of high CDK1 activity can trigger propagation of this state through the embryo from the site of ERK activation (Figure 1A).

Synchrony of cleavages is disrupted by alanine substitutions of Cdc25 phosphosites

As phosphoproteomic experiments suggest that Cdc25 (Stg) is a direct target of ERK activation, we sought to investigate the effects of ERK-dependent phosphosites in Stg by expressing an alanine-substituted mutant *in vivo*. We have identified four serines (S68, S76, S80, and S217) in Stg as high-confidence ERK-dependent phosphosites from our phosphoproteomics data (Figure 4A; Table S1). Based on this, we hypothesized that a mutant form of $Stg^{S68A,\ S76A,\ S80A,\ and\ S217A}$ (Stg-4A) would slow down cell-cycle progression in the early embryo.

To test this hypothesis, we first synthesized Stg-WT and Stg-4A mRNA by *in vitro* transcription and microinjected the mRNA into 0- to 30-min-old histone-mIFP embryos through the posterior (Figure 4A). Time-lapse imaging shows that 62.5% of the embryos (n = 8) injected with Stg-WT undergo one extra mitosis in either the whole embryo or in the posterior region (Figure 4B; Video S3). This is consistent with the notion that Stg acts as a limiting component that promotes cell-cycle progression by activating CDK1.[25,37] In contrast, in a third of embryos (n = 6) injected with Stg-4A, the mitotic waves from both poles slowed down and failed to spread across the entire embryo, leaving the nuclei arrested in interphase of NC12 or NC13 (Figure 4C; Video S3).

Given that many factors, including the amount of RNA and the injection positions, could contribute to the outcome of this injection experiment, localized expression of Stg transgene in the posterior of the embryo could be a less invasive way of testing whether the alanine-substituted mutant form of Stg modulates cell cycles. To achieve this, we expressed Stg-WT or Stg-4A with *nos* 5′ UTR and *nos* 3′ UTR under the control of the *nos* promoter (Figure 4D). The *nos* mRNA localizes at the posterior pole of the embryo and functions as a posterior determinant.[38] Adding the *nos* 3′ UTR to our Stg variants localizes them to the posterior pole of the embryo (Figure 4D).

Most embryos (80%, n = 15) derived from mothers with two copies of the Stg-WT transgene exhibited normal nuclear cycles and gastrulation (Figure 4E; Video S4). In contrast, ∼40% of Stg-4A embryos formed a successful blastoderm and gastrulated (n = 13). Interestingly, the rest of Stg-4A embryos either failed to form a blastoderm or exhibited nuclear cycles that lagged at the posterior region (Figure 4F; Video S4). Thus, posteriorly expressed Stg-4A is sufficient to delay nuclear-cycle progression. Taken together, these results show that ERK-dependent phosphorylation of Stg promotes the induction and propagation of mitotic entry.

Computational analysis indicates distributed control of embryonic cleavages by ERK

As tempting as it may be to assign the observed effects to the extensively studied Cdc25/Wee1/Cdk1 circuit,[15,39,40] it is likely to be only part of the whole story. For instance, our phosphoproteomic data suggest that ERK signaling is connected to other critical events of the cell cycle, such as nuclear envelope breakdown and kinetochore attachments (Figure 4G).[41,42] Bioinformatic analysis also suggests a widespread phosphoproteomic response.

ERK recognizes its substrates by interacting with their linear phosphorylation motifs and distal docking sites.[31,43] Consistent with this, the upregulated phosphoproteome, following 10 min of optoSos activation, was significantly enriched for proteins phosphorylated on ERK consensus motifs and containing docking sites (Figure 3C; Table S1). Among such proteins are several known ERK substrates, such as Nup153, which forms part of the nuclear pore complex and whose phosphorylation reduces its affinity for importin[44]; MED1, a subunit of the transcriptional coactivator mediator and whose phosphorylation promotes its interaction with the mediator complex[45]; and stathmin (STMN1), whose effects on microtubule dynamics are modulated upon phosphorylation.[46] However, many of the phosphosites (1,028 out 1,181) upregulated by a pulse of optoSos come from proteins that do not meet the criteria above (ERK phosphorylation motif and a docking site). Moreover, 178 phosphosites were significantly reduced in abundance, similar to what we have already demonstrated for the inhibitory sites in Cdk1 (Figure 3C). Thus, a significant fraction of these phosphorylation changes appear to be due to the indirect effects of ERK activation.

We used a computational strategy to assess the effects of additional phosphoregulators. This strategy is based on the phosphorylation site position weight matrices (PWMs) of human Ser/Thr kinases[30] (Figure S3A). We focused on the cytoplasmic Ser/Thr kinases expressed in nuclear cycle 14 *Drosophila* embryos (Table S1) and matched their PWMs to all the phosphosites (up/downregulated and static) in our data. Following the

Figure 4. ERK-dependent phosphorylation of Cdc25 (Stg) modulates mitotic entry

(A) Left: schematic of the Stg expression constructs for the mRNA injection experiments. Right: image showing the injection position.

(B and C) Still images from time-lapse imaging of embryos (Video S3) injected with Stg-WT or Stg-4A mRNA. Scale bars, 50 μm. (B) Red dotted line denotes the boundary between NC14 and NC15. (C) Red dotted lines denote the boundary between NC14 and NC13; red arrows indicate NC12 nuclei.

(D) Schematic of constructs for experiments with the posteriorly targeted Stg. Right: schematic of the localized expression of Stg variants in the posterior of the embryo.

(E and F) Still images from time-lapse imaging of embryos (Video S4) laid by females with two copies of *nos*:Stg-WT or *nos*:Stg-4A. Scale bars, 50 μm. (F) Red dotted line denotes the boundary between NC13 and NC12.

(G) Regulators of nuclear envelope breakdown and mitotic spindle assembly exhibit phosphorylation changes following 10 min optoSos. Regulatory relationships are based on *The Cell Cycle: Principles of Control*.[15] Gene Ontology (GO) enrichment analysis of the parent proteins of upregulated phosphosites using g:Profiler.[36] p values are Benjamini-Hochberg adjusted.

(H) A revised model for the biological effects of the first wave of ERK activation in *Drosophila*.

See also Table S1 and Videos S3 and S4.

approach described elsewhere,[30] this analysis revealed 3,796 high-quality matches to at least one of the 56 expressed kinases (Figure S3B). Next, we established that the activities of at least half of these kinases are significantly enriched over the background model of the predicted targets within the possible phosphoproteome derived from expressed proteins at this point in embryogenesis (Figure S3C).

Although ERK was among the list of kinases with enriched activity, its rank (11) was not as high as those of CDK1 (rank 1), a kinase that controls mitotic entry, and CDK7 (rank 4), a kinase that is involved in transcription initiation (Figure S3C). The high activity of these kinases is not surprising, since the embryo is completing rapid cleavage divisions and is about to start a major wave of zygotic gene activation. Finally, we asked which kinases' activities are significantly perturbed by activating optoSos (Figure S3D). Once again, ERK was not the only kinase that appeared to be activated by optoSos. The other significantly affected kinases include those that control cell cycle (CDK6), DNA damage responses (VRK1 and CHK2), transcription (CDK7, CDK8, and CDK9), and cell growth and metabolism (LKB1, p70S6K, and PAK1). These results offer a glimpse of a complex phosphoregulation network.

DISCUSSION

Our results reveal that functional effects of the first pulse of ERK signaling in the embryo are broader than the spatially restricted control of genes needed to form the terminal structures of the larva. In addition to acting through a handful of transcription factors identified by genetic studies, ERK activation at the poles is rapidly broadcast to the entire embryo through a vast network that includes both direct ERK substrates and phosphorylation cascades (Figure 4H). Although many of the candidate effectors responding to our optogenetic stimuli have been studied in cultured cells,[28,29] our work sets the stage for dissecting their individual and collective functions in a developmental context. As a first step in this direction, we used ectopic optogenetic activation and traditional loss-of-function approaches to demonstrate that ERK signaling at the poles ensures sychrony of embryonic cleavages.

The presented approach to functional analysis of phosphorylation networks should be applicable to a wide range of developmental and physiological contexts. To make the most of the emerging datasets, comprising large-scale changes in the abundance of phosphosites, it is critical to establish tools for delineating causal connections in phosphorylation networks.[47] The scale of the problem can be appreciated by considering the phosphoproteome of our experimental system, the fly embryo at the end of cleavage divisions, when about a third of the expressed proteins are phosphorylated, with some proteins carrying dozens of phosphosites. The first task is to understand how the observed phosphoproteome is established by the expressed kinases and phosphatases. Although recent assembly of kinase specificity matrices and docking sites provides an important component in completing this task,[30,31] it remains difficult to differentiate the targets of closely related kinases and to validate the large-scale predictions of the causal enzyme/substrate connections.[28] This task can be accomplished by analyzing how the phosphoproteome responds to acute perturbations of network components. Rapid progress of optogenetics that enables the delivery of increasingly precise stimuli should ultimately reveal how large-scale phosphorylation networks respond to both external cues and mutations.

Limitations of the study

In our phosphoproteomic experiments, SPS-MS3 data-dependent acquisition is inherently limited to detection of relatively high-abundance peptides, therefore missing lower-abundance phosphopeptides that may be differentially regulated between our samples. Another factor impacting depth is the challenge of collecting large numbers of embryos while adhering to the timing constraints of acute optogenetic treatments. Moreover, while our results suggest that ERK promotes mitotic entry, our bioinformatics analysis using kinase specificity matrices showed that Cdk1 activity was not significantly increased by optoSos. The similarities between ERK and Cdk1 consensus motifs pose a challenge in assigning phosphosites to one kinase or the other.

RESOURCE AVAILABILITY

Lead contact

Further information and requests for the resources and reagents should be directed to and will be fulfilled by the lead contact, Stanislav Y. Shvartsman (stas@princeton.edu).

Materials availability

Materials or fly strains available upon request from the lead contact.

Data and code availability

- All mass spectrometry proteomics data have been deposited to the ProteomeXchange Consortium via the PRIDE partner repository[50] with the dataset identifier PXD043371.
- All of the code used in the analyses is publicly available at GitHub (at: https://github.com/ddenberg/Mitotic-Wave-Classification DOI: https://doi.org/10.5281/zenodo.12832660 and https://github.com/Singh-Lab/optosos_supp_figures/tree/main DOI: https://doi.org/10.5281/zenodo.12837893)

ACKNOWLEDGMENTS

We would like to thank Trudi Schüpbach, Eric Wieschaus, Norbert Perrimon, Mariana Wolfner, David Morgan, Natalie Ahn, Jared Toettcher, Liz Gavis, and the members of the laboratory of S.Y.S. for helpful discussions. We thank Trudi Schüpbach, Eric Wieschaus, and Liz Gavis for sharing reagents used in this work and Eyan Yeung for contributions to the proteomic analysis during the early stages of our research. We also acknowledge support from the CCBX program of the Center for Computational Biology of the Flatiron Institute. Imaging was performed with support from the Confocal Imaging Facility, a Nikon Center of Excellence, in the Department of Molecular Biology at Princeton University, with assistance from Gary Laevsky and Sha Wang. We also thank Emily Ho and Sarah McFann for helpful suggestions on optogenetic experiments. The research was supported by Princeton Catalysis Initiative (M.W. and S.Y.S.), Bioengineering Initiative: Collaboration Proposal (M.W., S.Y.S and M.S.) NIH Research grants R35GM128813 (M.W.), R01HD085870 (S.Y.S.), R01GM141843 (A.V. and S.Y.S.), and R01GM134204 (S.Y.S.).

AUTHOR CONTRIBUTIONS

L.Y., A.Z., M.W., M.S., and S.Y.S. conceived and designed the study, with insight from R.A.M. and A.V. L.Y., A.Z., J.M.A., D.D., M.D.K., and A.N.T.J. performed experiments and analyzed data. L.Y., A.Z., J.M.A., M.W., M.S., and S.Y.S. wrote the manuscript.

DECLARATION OF INTERESTS

The authors declare no competing interests.

STAR★METHODS

Detailed methods are provided in the online version of this paper and include the following:

- KEY RESOURCES TABLE
- EXPERIMENTAL MODEL AND STUDY PARTICIPANT DETAILS
  - Drosophila strains
- METHOD DETAILS
  - Embryo collection
  - Immunostaining
  - Cloning and making transgenic flies
  - Preparation of RNAs and Microinjection
  - Microscopy
  - Interphase and M-phase classification
  - Sample preparation for phosphoproteomics
  - Embryo lysis and protein digestion
  - Tandem Mass Tag labeling
  - Phosphopeptide enrichment
  - Sample preparation for identifying the nuclear cycle 14 proteome
  - Fractionation of peptides
  - Liquid Chromatography and Mass Spectrometry
  - LC-MS/MS for phosphopeptides
  - LC-MS/MS for NC14 proteome
- QUANTIFICATION AND STATISTICAL ANALYSIS
  - Cell cycle analysis
  - Quantitative phosphoproteomic data processing
  - Inferring kinase activity
  - z-test statistic on kinase activity
  - Kinase match enrichment

SUPPLEMENTAL INFORMATION

Supplemental information can be found online at https://doi.org/10.1016/j.devcel.2024.08.004.

Received: October 31, 2023
Revised: June 13, 2024
Accepted: August 5, 2024
Published: August 28, 2024

REFERENCES

1. Avery, L., and Wasserman, S. (1992). Ordering gene function: the interpretation of epistasis in regulatory hierarchies. Trends Genet. *8*, 312–316. https://doi.org/10.1016/0168-9525(92)90263-4.
2. Wiese, K.E., Nusse, R., and van Amerongen, R. (2018). Wnt signalling: conquering complexity. Development *145*, dev165902. https://doi.org/10.1242/dev.165902.
3. Wieschaus, E., and Nüsslein-Volhard, C. (2016). The Heidelberg Screen for Pattern Mutants of Drosophila: A Personal Account. Annu. Rev. Cell Dev. Biol. *32*, 1–46. https://doi.org/10.1146/annurev-cellbio-113015-023138.
4. Friedman, A.A., Tucker, G., Singh, R., Yan, D., Vinayagam, A., Hu, Y., Binari, R., Hong, P., Sun, X., Porto, M., et al. (2011). Proteomic and functional genomic landscape of receptor tyrosine kinase and ras to extracellular signal-regulated kinase signaling. Sci. Signal. *4*, rs10. https://doi.org/10.1126/scisignal.2002029.
5. Smits, C.M., and Shvartsman, S.Y. (2020). The design and logic of terminal patterning in Drosophila. Curr. Top. Dev. Biol. *137*, 193–217. https://doi.org/10.1016/bs.ctdb.2019.11.008.
6. Farrell, J.A., and O'Farrell, P.H. (2014). From egg to gastrula: how the cell cycle is remodeled during the Drosophila mid-blastula transition. Annu. Rev. Genet. *48*, 269–294. https://doi.org/10.1146/annurev-genet-111212-133531.
7. Brantley, S.E., and Di Talia, S. (2021). Cell cycle control during early embryogenesis. Development *148*, dev193128. https://doi.org/10.1242/dev.193128.
8. Deneke, V.E., Puliafito, A., Krueger, D., Narla, A.V., De Simone, A., Primo, L., Vergassola, M., De Renzis, S., and Di Talia, S. (2019). Self-Organized Nuclear Positioning Synchronizes the Cell Cycle in Drosophila Embryos. Cell *177*, 925–941.e17. https://doi.org/10.1016/j.cell.2019.03.007.
9. Vergassola, M., Deneke, V.E., and Di Talia, S. (2018). Mitotic waves in the early embryogenesis of Drosophila: Bistability traded for speed. Proc. Natl. Acad. Sci. USA *115*, E2165–E2174. https://doi.org/10.1073/pnas.1714873115.
10. Di Talia, S., and Vergassola, M. (2022). Waves in Embryonic Development. Annu. Rev. Biophys. *51*, 327–353. https://doi.org/10.1146/annurev-biophys-111521-102500.
11. Su, T.T., Campbell, S.D., and O'Farrell, P.H. (1999). Drosophila grapes/CHK1 mutants are defective in cyclin proteolysis and coordination of mitotic events. Curr. Biol. *9*, 919–922. https://doi.org/10.1016/s0960-9822(99)80399-6.
12. Stumpff, J., Duncan, T., Homola, E., Campbell, S.D., and Su, T.T. (2004). Drosophila Wee1 kinase regulates Cdk1 and mitotic entry during embryogenesis. Curr. Biol. *14*, 2143–2148. https://doi.org/10.1016/j.cub.2004.11.050.
13. Yuan, K., Seller, C.A., Shermoen, A.W., and O'Farrell, P.H. (2016). Timing the Drosophila Mid-Blastula Transition: A Cell Cycle-Centered View. Trends Genet. *32*, 496–507. https://doi.org/10.1016/j.tig.2016.05.006.
14. Shindo, Y., and Amodeo, A.A. (2021). Excess histone H3 is a competitive Chk1 inhibitor that controls cell-cycle remodeling in the early Drosophila embryo. Curr. Biol. *31*, 2633–2642.e6. https://doi.org/10.1016/j.cub.2021.03.035.
15. Morgan, D.O. (2007). The Cell Cycle: Principles of Control (Published by New Science Press in Association with Oxford University Press. Distributed inside North America by Sinauer Associates, Publishers (New science press).
16. Deneke, V.E., Melbinger, A., Vergassola, M., and Di Talia, S. (2016). Waves of Cdk1 Activity in S Phase Synchronize the Cell Cycle in *Drosophila* Embryos. Dev. Cell *38*, 399–412. https://doi.org/10.1016/j.devcel.2016.07.023.
17. Wang, R., He, G., Nelman-Gonzalez, M., Ashorn, C.L., Gallick, G.E., Stukenberg, P.T., Kirschner, M.W., and Kuang, J. (2007). Regulation of Cdc25C by ERK-MAP kinases during the G2/M transition. Cell *128*, 1119–1132. https://doi.org/10.1016/j.cell.2006.11.053.
18. Casanova, J., and Struhl, G. (1993). The torso receptor localizes as well as transduces the spatial signal specifying terminal body pattern in Drosophila. Nature *362*, 152–155. https://doi.org/10.1038/362152a0.
19. Futran, A.S., Link, A.J., Seger, R., and Shvartsman, S.Y. (2013). ERK as a model for systems biology of enzyme kinetics in cells. Curr. Biol. *23*, R972–R979. https://doi.org/10.1016/j.cub.2013.09.033.
20. Doherty, C.A., Diegmiller, R., Kapasiawala, M., Gavis, E.R., and Shvartsman, S.Y. (2021). Coupled oscillators coordinate collective germline growth. Dev. Cell *56*, 860–870.e8. https://doi.org/10.1016/j.devcel.2021.02.015.
21. Goyal, Y., Schüpbach, T., and Shvartsman, S.Y. (2018). A quantitative model of developmental RTK signaling. Developmental Biology *442*, 80–86. https://doi.org/10.1016/j.ydbio.2018.07.012.
22. Toettcher, J.E., Weiner, O.D., and Lim, W.A. (2013). Using optogenetics to interrogate the dynamic control of signal transmission by the Ras/Erk module. Cell *155*, 1422–1434. https://doi.org/10.1016/j.cell.2013.11.004.
23. Johnson, H.E., Djabrayan, N.J.V., Shvartsman, S.Y., and Toettcher, J.E. (2020). Optogenetic Rescue of a Patterning Mutant. Curr. Biol. *30*, 3414–3424.e3. https://doi.org/10.1016/j.cub.2020.06.059.
24. Hayden, L., Chao, A., Deneke, V.E., Vergassola, M., Puliafito, A., and Di Talia, S. (2022). Cullin-5 mutants reveal collective sensing of the

nucleocytoplasmic ratio in Drosophila embryogenesis. Curr. Biol. *32*, 2084–2092.e4. https://doi.org/10.1016/j.cub.2022.03.007.

25. Di Talia, S., She, R., Blythe, S.A., Lu, X., Zhang, Q.F., and Wieschaus, E.F. (2013). Posttranslational control of Cdc25 degradation terminates Drosophila's early cell-cycle program. Curr. Biol. *23*, 127–132. https://doi.org/10.1016/j.cub.2012.11.029.

26. Edgar, B.A., Lehman, D.A., and O'Farrell, P.H. (1994). Transcriptional regulation of string (cdc25): a link between developmental programming and the cell cycle. Development *120*, 3131–3143. https://doi.org/10.1242/dev.120.11.3131.

27. Alphey, L., Jimenez, J., White-Cooper, H., Dawson, I., Nurse, P., and Glover, D.M. (1992). twine, a cdc25 homolog that functions in the male and female germline of Drosophila. Cell *69*, 977–988. https://doi.org/10.1016/0092-8674(92)90616-k.

28. Ünal, E.B., Uhlitz, F., and Blüthgen, N. (2017). A compendium of ERK targets. FEBS Lett. *591*, 2607–2615. https://doi.org/10.1002/1873-3468.12740.

29. Klomp, J.E., Diehl, J.N., Klomp, J.A., Edwards, A.C., Yang, R., Morales, A.J., Taylor, K.E., Drizyte-Miller, K., Bryant, K.L., Schaefer, A., et al. (2024). Determining the ERK-regulated phosphoproteome driving KRAS-mutant cancer. Science *384*, eadk0850. https://doi.org/10.1126/science.adk0850.

30. Johnson, J.L., Yaron, T.M., Huntsman, E.M., Kerelsky, A., Song, J., Regev, A., Lin, T.Y., Liberatore, K., Cizin, D.M., Cohen, B.M., et al. (2023). An atlas of substrate specificities for the human serine/threonine kinome. Nature *613*, 759–766. https://doi.org/10.1038/s41586-022-05575-3.

31. Arur, S., Ohmachi, M., Nayak, S., Hayes, M., Miranda, A., Hay, A., Golden, A., and Schedl, T. (2009). Multiple ERK substrates execute single biological processes in Caenorhabditis elegans germ-line development. Proc. Natl. Acad. Sci. USA *106*, 4776–4781. https://doi.org/10.1073/pnas.0812285106.

32. Patel, A.L., Zhang, L., Keenan, S.E., Rushlow, C.A., Fradin, C., and Shvartsman, S.Y. (2021). Capicua is a fast-acting transcriptional brake. Curr. Biol. *31*, 3703. https://doi.org/10.1016/j.cub.2021.07.045.

33. Jiménez, G., Shvartsman, S.Y., and Paroush, Z. (2012). The Capicua repressor–a general sensor of RTK signaling in development and disease. J. Cell Sci. *125*, 1383–1391. https://doi.org/10.1242/jcs.092965.

34. Keenan, S.E., Blythe, S.A., Marmion, R.A., Djabrayan, N.J.V., Wieschaus, E.F., and Shvartsman, S.Y. (2020). Rapid Dynamics of Signal-Dependent Transcriptional Repression by Capicua. Dev. Cell *52*, 794–801.e4. https://doi.org/10.1016/j.devcel.2020.02.004.

35. Kim, S.Y., Song, E.J., Lee, K.J., and Ferrell, J.E., Jr. (2005). Multisite M-phase phosphorylation of Xenopus Wee1A. Mol. Cell. Biol. *25*, 10580–10590. https://doi.org/10.1128/MCB.25.23.10580-10590.2005.

36. Raudvere, U., Kolberg, L., Kuzmin, I., Arak, T., Adler, P., Peterson, H., and Vilo, J. (2019). g:Profiler: a web server for functional enrichment analysis and conversions of gene lists (2019 update). Nucleic Acids Res. *47*, W191–W198. https://doi.org/10.1093/nar/gkz369.

37. Coleman, T.R., and Dunphy, W.G. (1994). Cdc2 regulatory factors. Curr. Opin. Cell Biol. *6*, 877–882. https://doi.org/10.1016/0955-0674(94)90060-4.

38. Forrest, K.M., Clark, I.E., Jain, R.A., and Gavis, E.R. (2004). Temporal complexity within a translational control element in the nanos mRNA. Development *131*, 5849–5857. https://doi.org/10.1242/dev.01460.

39. Trunnell, N.B., Poon, A.C., Kim, S.Y., and Ferrell, J.E., Jr. (2011). Ultrasensitivity in the Regulation of Cdc25C by Cdk1. Mol. Cell *41*, 263–274. https://doi.org/10.1016/j.molcel.2011.01.012.

40. Pomerening, J.R., Sontag, E.D., and Ferrell, J.E., Jr. (2003). Building a cell cycle oscillator: hysteresis and bistability in the activation of Cdc2. Nat. Cell Biol. *5*, 346–351. https://doi.org/10.1038/ncb954.

41. Shapiro, P.S., Vaisberg, E., Hunt, A.J., Tolwinski, N.S., Whalen, A.M., McIntosh, J.R., and Ahn, N.G. (1998). Activation of the MKK/ERK pathway during somatic cell mitosis: direct interactions of active ERK with kinetochores and regulation of the mitotic 3F3/2 phosphoantigen. J. Cell Biol. *142*, 1533–1545. https://doi.org/10.1083/jcb.142.6.1533.

42. Mulner-Lorillon, O., Chassé, H., Morales, J., Bellé, R., and Cormier, P. (2017). MAPK/ERK activity is required for the successful progression of mitosis in sea urchin embryos. Dev. Biol. *421*, 194–203. https://doi.org/10.1016/j.ydbio.2016.11.018.

43. Futran, A.S., Kyin, S., Shvartsman, S.Y., and Link, A.J. (2015). Mapping the binding interface of ERK and transcriptional repressor Capicua using photocrosslinking. Proc. Natl. Acad. Sci. USA *112*, 8590–8595. https://doi.org/10.1073/pnas.1501373112.

44. Kosako, H., Yamaguchi, N., Aranami, C., Ushiyama, M., Kose, S., Imamoto, N., Taniguchi, H., Nishida, E., and Hattori, S. (2009). Phosphoproteomics reveals new ERK MAP kinase targets and links ERK to nucleoporin-mediated nuclear transport. Nat. Struct. Mol. Biol. *16*, 1026–1035. https://doi.org/10.1038/nsmb.1656.

45. Belakavadi, M., Pandey, P.K., Vijayvargia, R., and Fondell, J.D. (2008). MED1 phosphorylation promotes its association with mediator: implications for nuclear receptor signaling. Mol. Cell. Biol. *28*, 3932–3942. https://doi.org/10.1128/MCB.02191-07.

46. Filbert, E.L., Le Borgne, M., Lin, J., Heuser, J.E., and Shaw, A.S. (2012). Stathmin regulates microtubule dynamics and microtubule organizing center polarization in activated T cells. J. Immunol. *188*, 5421–5427. https://doi.org/10.4049/jimmunol.1200242.

47. Needham, E.J., Parker, B.L., Burykin, T., James, D.E., and Humphrey, S.J. (2019). Illuminating the dark phosphoproteome. Sci. Signal. *12*, eaau8645. https://doi.org/10.1126/scisignal.aau8645.

48. Johnson, H.E., Goyal, Y., Pannucci, N.L., Schüpbach, T., Shvartsman, S.Y., and Toettcher, J.E. (2017). The Spatiotemporal Limits of Developmental Erk Signaling. Dev. Cell *40*, 185–192. https://doi.org/10.1016/j.devcel.2016.12.002.

49. Schindelin, J., Arganda-Carreras, I., Frise, E., Kaynig, V., Longair, M., Pietzsch, T., Preibisch, S., Rueden, C., Saalfeld, S., Schmid, B., et al. (2012). Fiji: an open-source platform for biological-image analysis. Nat. Methods *9*, 676–682. https://doi.org/10.1038/nmeth.2019.

50. Perez-Riverol, Y., Csordas, A., Bai, J.W., Bernal-Llinares, M., Hewapathirana, S., Kundu, D.J., Inuganti, A., Griss, J., Mayer, G., Eisenacher, M., et al. (2019). The PRIDE database and related tools and resources in 2019: improving support for quantification data. Nucleic Acids Res. *47*, D442–D450. https://doi.org/10.1093/nar/gky1106.

51. Goyal, Y., Jindal, G.A., Pelliccia, J.L., Yamaya, K., Yeung, E., Futran, A.S., Burdine, R.D., Schüpbach, T., and Shvartsman, S.Y. (2017). Divergent effects of intrinsically active MEK variants on developmental Ras signaling. Nat. Genet. *49*, 465–469. https://doi.org/10.1038/ng.3780.

52. Eagle, W.V.I., Yeboah-Kordieh, D.K., Niepielko, M.G., and Gavis, E.R. (2018). Distinct cis-acting elements mediate targeting and clustering of Drosophila polar granule mRNAs. Development *145*, dev164657. https://doi.org/10.1242/dev.164657.

53. Gupta, M., Sonnett, M., Ryazanova, L., Presler, M., and Wühr, M. (2018). Quantitative Proteomics of Xenopus Embryos I, Sample Preparation. Methods Mol. Biol. *1865*, 175–194. https://doi.org/10.1007/978-1-4939-8784-9_13.

54. Presler, M., Van Itallie, E., Klein, A.M., Kunz, R., Coughlin, M.L., Peshkin, L., Gygi, S.P., Wühr, M., and Kirschner, M.W. (2017). Proteomics of phosphorylation and protein dynamics during fertilization and meiotic exit in the Xenopus egg. Proc. Natl. Acad. Sci. USA *114*, E10838–E10847. https://doi.org/10.1073/pnas.1709207114.

55. McAlister, G.C., Nusinow, D.P., Jedrychowski, M.P., Wühr, M., Huttlin, E.L., Erickson, B.K., Rad, R., Haas, W., and Gygi, S.P. (2014). MultiNotch MS3 enables accurate, sensitive, and multiplexed detection of differential expression across cancer cell line proteomes. Anal. Chem. *86*, 7150–7158. https://doi.org/10.1021/ac502040v.

56. Johnson, A., Stadlmeier, M., and Wühr, M. (2021). TMTpro Complementary Ion Quantification Increases Plexing and Sensitivity for Accurate Multiplexed Proteomics at the MS2 Level. J. Proteome Res. *20*, 3043–3052. https://doi.org/10.1021/acs.jproteome.0c00813.

57. Chari, S., Wilky, H., Govindan, J., and Amodeo, A.A. (2019). Histone concentration regulates the cell cycle and transcription in early development. Development *146*, dev177402. https://doi.org/10.1242/dev.177402.

58. Benjamini, Y., and Hochberg, Y. (1995). Controlling the False Discovery Rate - a Practical and Powerful Approach to Multiple Testing. J. R. Stat. Soc. B *57*, 289–300. https://doi.org/10.1111/j.2517-6161.1995.tb02031.x.

59. Benjamini, Y., and Yekutieli, D. (2001). The control of the false discovery rate in multiple testing under dependency. Ann. Statist. *29*, 1165–1188. https://doi.org/10.1214/aos/1013699998.

60. Beausoleil, S.A., Villén, J., Gerber, S.A., Rush, J., and Gygi, S.P. (2006). A probability-based approach for high-throughput protein phosphorylation analysis and site localization. Nat. Biotechnol. *24*, 1285–1292. https://doi.org/10.1038/nbt1240.

61. Dephoure, N., Zhou, C., Villén, J., Beausoleil, S.A., Bakalarski, C.E., Elledge, S.J., and Gygi, S.P. (2008). A quantitative atlas of mitotic phosphorylation. Proc. Natl. Acad. Sci. USA *105*, 10762–10767. https://doi.org/10.1073/pnas.0805139105.

62. Ochoa, D., Jarnuczak, A.F., Viéitez, C., Gehre, M., Soucheray, M., Mateus, A., Kleefeldt, A.A., Hill, A., Garcia-Alonso, L., Stein, F., et al. (2020). The functional landscape of the human phosphoproteome. Nat. Biotechnol. *38*, 365–373. https://doi.org/10.1038/s41587-019-0344-3.

63. Hernandez-Armenta, C., Ochoa, D., Gonçalves, E., Saez-Rodriguez, J., and Beltrao, P. (2017). Benchmarking substrate-based kinase activity inference using phosphoproteomic data. Bioinformatics *33*, 1845–1851. https://doi.org/10.1093/bioinformatics/btx082.

Please cite this article in press as: Yang et al., ERK synchronizes embryonic cleavages in *Drosophila*, Developmental Cell (2024), https://doi.org/10.1016/j.devcel.2024.08.004

STAR★METHODS

KEY RESOURCES TABLE

REAGENT or RESOURCE	SOURCE	IDENTIFIER
Antibodies		
Donkey anti sheep, Alexa-488	Thermo Fisher Scientific	Cat # A-11015; RRID: AB_2534082
Phospho-p44/42 MAPK (Erk1/2) (Thr202/Tyr204)	Cell Signaling Technology	Cat # 4370; RRID: AB_2315112
Donkey polyclonal anti-rabbit Alexa 568 (1:500)	Invitrogen	Cat#A10042; RRID: AB_2534017
GFP sheep antibody	Bio-Rad	Cat # 4745-1051; RRID: AB_619712
Chemicals, peptides, and recombinant proteins		
Protease inhibitor cocktail	Roche	Cat#4693124001
PhosSTOP phosphatase inhibitor cocktail	Roche	Cat#4906837001
Lysyl Endopeptidase, mass spectrometry grade (Lys-C)	Wako Chemicals	Cat#125-05061
Sequencing grade modified Trypsin	Promega	Cat#PAV5113
TMTpro 16-plex	Thermo Fisher Scientific	Cat#A44520
DAPI	Invitrogen	Cat#D1306
Methanol	VWR	Cat#BDH1135
37% Formaldehyde solution	Fisher Scientific	Cat#F79-1
Heptane	Sigma	Cat#32287
PBS	Fisher Scientific	Cat#BP2944
Triton X-100	Fisher Scientific	Cat#X100
Tween-20	Sigma	Cat#P1379
Critical commercial assays		
Q5 site-directed mutagenesis kit	NEB	#E0554S
NEBuilder® HiFi DNA Assembly Master Mix	NEB	#E2621S
HiScribe ARCA mRNA kit	NEB	#E2060S
high pH reversed-phase peptide fractionation kit	Pierce	#84868
Deposited data		
Raw and processed mass spectrometry proteomics data	This paper	ProteomeXchange: PXD043371
The Kinase Library	Johnson et al.[30]	https://kinase-library.phosphosite.org
Experimental models: Organisms/strains		
D. melanogaster: HisGFP	Bloomington Drosophila Stock Center	Cat#5941
D. melanogaster: y[1] w[1118]	Bloomington Drosophila Stock Center	Cat#6598
D. melanogaster: UAS-optoSOS	Johnson et al.[48]	N/A
D. melanogaster: CycE-sfGFP	Doherty et al.[20]	N/A
D. melanogaster: mCherry-RNAi	Bloomington Drosophila Stock Center	Cat#35781
D. melanogaster: MTD-gal4	Bloomington Drosophila Stock Center	Cat#31777
D. melanogaster: MEK-RNAi1	Bloomington Drosophila Stock Center	Cat#35216
D. melanogaster: MEK-RNAi2	Bloomington Drosophila Stock Center	Cat#34830
D. melanogaster: 67;15	Bloomington Drosophila Stock Center	Cat#80361
D. melanogaster: his-miFP	Bloomington Drosophila Stock Center	Cat#95105
D. melanogaster: nos:Stg	This study	N/A
D. melanogaster: nos:Stg4A	This study	N/A
Oligonucleotides		
primer1	stg2pnosXnos_F	gtaactttcgacccggattttcgcc ATGCTGTGGGAAACTATTGTG

(*Continued on next page*)

Continued

REAGENT or RESOURCE	SOURCE	IDENTIFIER
primer2	stg2pnosXnos_R	gcctctgctccagagctggattcgc CTACAGCATCAGTCGCGAG
primer3	pnosXnos_F	GCGAATCCAGCTCTGGAG
primer4	pnosXnos_R	GGCGAAAATCCGGGTCGAAAG
primer5	stg_S68A_S76A_S80A_F	tgctcgcgccggagggcgcg CCCCAGCGCTTCCAG
primer6	stg_S68A_S76A_S80A_R	gacccatcagctccggagc GGCCGATCGCTGCTG
primer7	stg_S217A_F	GGCCAACTGCgcgCCCATCCAGA
primer8	stg_S217A_R	GATGCTGGCGGTTCCGGG
primer9	Stg_tubUTR_F	tggatcccccgggctgcaggcaac ATGCTGTGGGAAACTATTGTG
primer10	Stg_tubUTR_R	ggcgcgacgcttagttatcg CTACAGCATCAGTCGCGAG
Recombinant DNA		
BS09140	DGRC	DGRC_1633394
pBS-P_{nos}GFP	Elizabeth R. Gavis	N/A
pBS-SK(+)-ta3'UTR	Elizabeth R. Gavis	N/A
Software and algorithms		
Fiji	Schindelin et al.[49]	http://fiji.sc
MATLAB	Mathworks	https://www.mathworks.com
RStudio	Posit	https://posit.co/download/rstudio-desktop/
Python 3.10.7	Python Software Foundation	https://www.python.org/downloads/release/python-3107/
Interphase and M-phase classification	This study	DOI: https://doi.org/10.5281/zenodo.12832660
Inferring kinase activity	This study	DOI: https://doi.org/10.5281/zenodo.12837893

EXPERIMENTAL MODEL AND STUDY PARTICIPANT DETAILS

Drosophila strains

Fly stocks were maintained under standard conditions and all crosses were performed at 25°C except the crosses for RNAi experiments were kept at 27°C. $y^{[1]}w^{[1118]}$ (*yw*) (Bloomington #6598), HisGFP (Bloomington #5941), UAS-optoSOS,[48] CycE-sfGFP,[20] mat67 (Bloomington #80361), his3.3-mIFP (Bloomington #95105), mCherry-RNAi (Bloomington #35785), MTD-gal4 (Bloomington #31777), MEK-RNAi1 (Bloomington #35216), MEK-RNAi2 (Bloomington #34830), ovo^{D1}(Bloomington #1813), torso-RNAi (Bloomington #58312), mek^{LH110}, trk^2 and trk^3 (gifts from Trudi Schüpbach) lines were used in this study.

METHOD DETAILS

Embryo collection

For optoSOS experiments, crosses between female UAS-optoSOS flies and MTD-gal4 males were protected from room light. To collect embryos for phosphoproteomics or immunostaining, progenies of UAS-optoSOS flies and MTD-gal4 males were kept in cages with apple juice agar plates. 0-1 h old embryos were dechorionated with 50% bleach for 2 min. Dechorionated embryos were washed with water, and dried briefly. Half of the embryos were incubated in the dark for 2 h. The other half were incubated in the dark for 110 or 117 min, then illuminated with blue LEDs in an aluminum foil box for 10 min or 3min. After illumination, the embryos were flash frozen in liquid nitrogen for phosphoproteomic experiments, or fixed for immunostaining.

Immunostaining

dpERK antibody staining protocol was performed as described previously by Goyal et al.[51] Rabbit anti-dpERK (1:100; Cell Signaling Technology #4370S) was used as primary antibody. DAPI (1:10000; Molecular probes #D1306) was used to stain for nuclei, and donkey anti rabbit Alexa-568 (1:500; Invitrogen #A-10042) was used as secondary antibody.

Cloning and making transgenic flies

The plasmid pBS-P_{nos}-Stg-WT was created by substituting the GFP-*nos* coding region by the Stg CDS. In brief, full-length *stg* CDS was PCR amplified from BS09140 (DGRC Stock 1633394; https://dgrc.bio.indiana.edu//stock/1633394; RRID:DGRC_1633394) using primers (1) and (2). The pBS-P_{nos} backbone fragment was PCR amplified from the pBS-P_{nos}GFP plasmid[38] using primers (3) and (4). Then the Stg fragment and pBS-P_{nos} backbone fragment were used to generate pBS-P_{nos}-Stg-WT by two-piece Gibson assembly (NEB #E2621S). Then Q5 site-directed mutagenesis kit (NEB #E0554S) was used to generate pBS-P_{nos}-Stg-4A using primers (5) and (6), and primers (7) and (8). For creation of the transgenic flies expressing Stg-WT and Stg-4A, the pBS-P_{nos}-Stg-WT and pBS-P_{nos}-Stg-4A were injected into flies containing the *attP* site VK02 (BDSC #9723). Transgenesis was conducted by BestGene Inc.

Preparation of RNAs and Microinjection

Stg-WT and Stg-4A fragments were PCR amplified from pBS-P_{nos}-Stg-WT and pBS-P_{nos}-Stg-4A plasmids generated above using primers (9) and (10). Then the PCR fragments were inserted into the *EcorRI* site of pBS-SK(+)-ta3'UTR plasmid containing the tubulin 3'UTR sequence[52] to generate the pBS-SK-Stg-WT-*tub*3'UTR and pBS-SK-Stg-4A-*tub*3'UTR. For in vitro transcription, PCR fragments containing T3 promoter, Stg CDS variants (WT or 4A) and *tubulin* 3'UTR were amplified from pBS-stgWT-*tub*3'UTR or pBS-stg4A-*tub*3'UTR plasmid. Then, these PCR fragments were used as templates to synthesize mRNA for microinjection using T3 RNA polymerase (NEB #M0378S) and reagents from HiScribe ARCA mRNA kit (with tailing) (NEB #E2060S) following the manufacturer's instructions. Synthesized mRNA was precipitated and resuspended in nuclease-free water at 0.5 mg/mL.

his3.3-mIFP Embryos were collected on apple juice plates for 0.5 hr, hand-dechorionated, transferred to a coverslip with heptane glue, desiccated, and placed in Halocarbon oil 200. Embryos were then injected from the posterior with 1 pL of *Stg-WT* or *Stg-4A* mRNA at 0.5 mg/mL.

Microscopy

Fixed imaging for dpERK antibody staining was performed with an upright Leica SP5 confocal microscope with 20× air objectives using an argon ion laser and 405-nm and 561-nm lasers. For dpERK quantification, UAS-optoSOS embryos were mounted on the same slide with HisGFP embryos, and imaged at the midsagittal plane. dpERK quantification was described previously by Goyal et al.[51]

Embryonic cuticle preparation was described previously by Goyal et al.[51] Embryos were aged more than 24 hours before being dechorionated with 50% bleach. Then the embryos were shaken in methanol and heptane (1:1) and incubated in a media containing lactic acid and Hoyer's media at 65°C. Embryos were imaged on a Nikon Eclipse Ni in darkfield.

Live imaging for optoSOS; his3.3-mIFP was performed on a Nikon A1 RS confocal microscope with a 20× air objective using an 633-nm laser. Embryos from mat67/optoSOS; his3.3-mIFP/+ mothers were dechorionated with 50% bleach for 2 min, then mounted in water on a 35 mm coverslip dish (MatTek). A 20 μm-width stripe was illuminated using a Mightex Polygon digital micromirror device (DMD) with an X-cite XLED 450-nm blue light source. To visualize mitotic entry, embryos were illuminated for 0.1 s every 6 s and imaged every 6 s with a 561-nm laser, with z stacks taken from the embryo surface to a depth of 9 μm with a step size of 3 μm. To visualize cell cycle progression, embryos from WT or trk^2/trk^3 mothers were imaged every 15 s with a 561-nm laser, with z stacks taken from the embryo surface to a depth of 20 μm with a step size of 3 μm.

Live imaging for CycE-sfGFP embryos were performed with the Leica SP5 confocal microscope with 20× air objective. Embryos from CycE-sfGFP/Gal4; mCherry-RNAi/Gal4-VP16 or CycE-sfGFP/Gal4; MEK-RNAi/Gal4-VP16 mothers were dechorionated with 50% bleach for 2 min, then mounted in water on a 35 mm coverslip dish (MatTek). Images were acquired every 10 s with an argon laser, with z stacks taken from the embryo surface to a depth of 12 μm with a step size of 1.85 μm.

Live imaging for Stg variants-expressing embryos were performed with the Leica SP5 confocal microscope with 20× air objective. Embryos with injected mRNAs or from nos:StgWT/ nos:StgWT; his3.3-mIFP or nos:Stg4A/nos:Stg4A; his3.3-mIFP mothers were dechorionated with 50% bleach for 2 min, then mounted in water on a 35 mm coverslip dish (MatTek). Images were acquired every 10 s with an argon laser, with z stacks taken from the embryo surface to a depth of 20 μm with a step size of 2.85 μm.

Interphase and M-phase classification

The z stack sequences were first preprocessed in FIJI[49] using a summed z projection of pixel intensities. The pixel classification pipeline in ilastik was then used to train a probability map discriminating between nuclei and background pixels. Training was performed manually by labeling pixels belonging to each class using ilastik's interface. The probability maps were used as input to the watershed algorithm to perform instance segmentation of nuclei in MATLAB. To improve the quality of the segmented regions a Gaussian smoothing with a sigma of 0.5 was applied to the probability maps, followed by an H-maxima transform with a threshold of 0.5. The H-maxima transform was necessary to segment nuclei at later time points whose histone signal had decayed significantly.

Following segmentation, nuclei were categorized to be in 'interphase' or 'mitosis' at each frame of the sequence. Using ilastik's object classification pipeline, nuclei were manually labeled according to their shape and intensity. The output of ilastik produced temporal flickering artifacts between the two classes in the transitions between interphase and mitosis. Flickering was reduced by first tracking cells over time using TrackMate, and second computing the mode of each nuclei's class in a 5 frame moving window. Finally, kymographs were constructed by averaging the object classes along the DV-axis and along the AP-axis with a 15 pixel moving average, for each frame in the sequence.

Sample preparation for phosphoproteomics

Samples were prepared as previously described in previous works,[53,54] with minor modifications.

Embryo lysis and protein digestion

Frozen embryos were briefly thawed on ice and lysed by 5-8 volumes of lysis buffer (50 mM HEPES pH 7.2, 2% SDS, 5 mM EDTA) containing protease inhibitors (Roche #4693124001) and PhosStop phosphatase inhibitors (Roche #4906837001) in a glass homogenizer. All buffers were made with HPLC-grade water. Lysates were sonicated for 1 min and then clarified by centrifuge at 20,000 rcf at 4 °C. The samples were reduced with 5 mM DTT for 20 min at 60 °C. Cysteines were alkylated with 15 mM N-ethylmaleimide (NEM) for 20 min at room temperature (RT). Excess NEM was reacted away with an additional 5 mM DTT at RT. Proteins were precipitated by methanol/chloroform. The protein pellet was resuspended in 6 M guanidine HCl and 50 mM 3-[4-(2-hydroxyethyl)-1-piperazinyl]-propanesulfonic acid (EPPS), pH 8.5, with gentle pipetting and heated to 60 °C for 5 min. The protein concentration was quantified by BCA assay, and adjusted to ~4 mg/mL. Eight repeats for each of the 10 min light or dark conditions were used for further steps. For ~400 μg of protein per condition, samples were diluted to 2 M guanidine with 10 mM EPPS, pH 8.5, and digested with Lys-C (Wako Chemicals) at 20 ng/μL at RT overnight. Next, samples were diluted to 0.5 M guanidine HCl with 10 mM EPPS, pH 8.5, and digested further by adding 20 ng/μL of Lys-C and 10 ng/μL of sequencing grade trypsin (Promega). Digestions were incubated at 37 °C overnight. Digested peptides were quantified with a colorimetric peptide assay (Pierce #23275). 100 μg of peptides per replicate were dried in a SpeedVac.

Tandem Mass Tag labeling

Dried peptides from digestion were labeled using 16-plex tandem mass tag (TMTpro) reagents (Thermo Fisher Scientific #A44520) for 10 min optoSos, and 18-plex TMTpro reagents (Thermo Fisher Scientific #A52045) for 3 min optoSos. 100 μg of dried peptides were resuspended with 100 μL of 200 mM EPPS, pH 8.0. 40 μL of TMTpro stock solution (20 μg/μL in dry acetonitrile) was added to each sample and incubated at RT for 2 h. The reaction was quenched by 10 mM hydroxylamine at RT for 15 min. All conditions were combined in one tube, and were acidified by addition of phosphoric acid to 5%. Samples were clarified by spinning at 20,000 rcf for 20 min. Sep-Pak C18 solid-phase extraction (50 mg) (Waters #WAT054955) was used to desalt and isolate peptides.

Phosphopeptide enrichment

TMTpro-labeled peptides were resuspended in 0.5 mL of 2 M lactic acid / 50% acetonitrile (ACN) and centrifuged at 20,000 g for 30 min. Supernatant was transferred to an Eppendorf tube containing 8 mg of titanium dioxide beads (GL Sciences #5020-75000), and vortexed for 1 h at RT. A 0.22 μm PTFE membrane filter unit (Millipore #UFC30LG25) was used to filter the titanium dioxide beads. The first flowthrough was collected for a second enrichment. The beads were washed three times with 2 M lactic acid / 50% ACN, and twice with 0.1% TFA in 25% ACN. The phosphopeptides were eluted with 1.2 mL of 200 mM KH2PO4, pH 10. The second enrichment was performed as above, and the second flowthrough was saved for non-phosphopeptide quantification. ~4 μg of peptides from each enrichment was analyzed by LC-MS (nLC-1200 HPLC; Orbitrap Fusion Lumos) using a MS3 synchronous precursor selection method.[55] The remaining sample was fractionated using a high pH reversed-phase peptide fractionation kit (Pierce #84868) and analyzed by LC-MS.

Sample preparation for identifying the nuclear cycle 14 proteome

For obtaining the NC14 proteome, 900μL of lysis solution (50mM HEPES pH 7.2, 2% SDS, 1x protease inhibitor) was then added to 1330 embryos. The embryos were lysed by tip-sonicating with 50% power, 10 seconds on, 20 seconds off, 10 times. The protein lysate was prepared as above, and the protein concentration was adjusted to ~5 mg/mL in 6 M guanidine HCl with 50 mM EPPS, pH 8.5. ~160 μg of protein was used for sample preparation. The sample underwent Lys-C/Trypsin digestion as above. Salt and undigested proteins were removed by C18 solid-phase extraction (50 mg) (SepPak; Waters). The sample was dried in a SpeedVac overnight.

Fractionation of peptides

Dried peptides from digestion were resuspended in 10mM ammonium bicarbonate pH 8.0 then fractionated by medium pH reverse-phase HPLC (Aligent 1220 LC) using a flow rate of 0.5 mL/min throughout. The gradient was 0% acetonitrile for 18 minutes, then 7% acetonitrile to 35% for 57 minutes; then, a flat gradient of 95% acetonitrile was applied for 5 minutes. The fractions were collected using a fraction collector (Aligent 1260 Infinity) into a 96 well plate. The 96 fractions were pooled into 24 fractions by combining the alternating well from each column of the plate. Each fraction was dried in a SpeedVac and resuspended in 50 μL of 5% phosphoric acid. Stage-tip was performed to desalt the sample, and the sample was resuspended in 6 μL of 1% formic acid. Approximated 1.5 μL was analyzed by LC-MS.

Liquid Chromatography and Mass Spectrometry

All samples were analyzed on a Proxeon nLC-1200 HPLC coupled to a Thermo Scientific Orbitrap Fusion Lumos mass spectrometer.

LC-MS/MS for phosphopeptides

Phosphopeptides were separated on an Aurora Gen 3 Ultimate nanoflow UHPLC column (25 cm x 75 μm ID, 1.7 μm C18). Solvent A consisted of 2% DMSO, 0.125% formic acid in water, solvent B of 80% MeCN, 2% DMSO and 0.125% formic acid in water. The following gradient with percentage of solvent B was applied at a constant flow rate of 350 nL/min: 0%–8% for 5 min; 8%–24% for 150 min (unfractionated) or 65 min (fractionated); 24%–60% for 15 min (unfractionated) or 10 min (fractionated); 60%–100% for 5 min; and 100% for 5 min. For electrospray ionization, 2.6 kV were applied from 1-175 min (unfractionated) or 1-85 min (fractionated) of the gradient through the column. The mass spectrometer was set to analyze positively charged ions in a data-dependent SPS-MS3 mode, recording centroid data with an RF lens level of 20% and the following full scan properties: Orbitrap detector, AGC target of 4E5 charges, maximum ion injection time of 10 ms, scan range m/z 350-1500 with quadrupole isolation, and 120k resolution. For triggering MS2 scans, monoisotopic peak determination was set to "peptide mode", and charge states 2 – 6 were included for analysis. The dynamic exclusion duration was set to 60 s (unfractionated) or 30 s (fractionated) with a +/- 10 ppm mass tolerance window. For the MS2 analysis in the ion trap, the AGC target was set to 1E4 charges. Ions were selected with a 0.5 m/z isolation window and fragmented with a CID collision energy of 35%. After MS2 acquisition, MS3 scans were triggered using the following filters: Exclusion mass width of 70 m/z (low) and 5 m/z (high); TMTpro Isobaric Tag Loss Exclusion. MS3 precursors were fragmented with an HCD collision energy of 45% in the Orbitrap. The MS isolation window was 1.2 m/z and the MS2 isolation window was 2 m/z. The AGC target was set to 1E5 charges, and the scan range was set to 110-140 m/z. Additional settings were as previously described by Johnson et al.[56]

LC-MS/MS for NC14 proteome

The HPLC was set to 350 nL/min flowrate with a gradient from 0% B to 10% B for the first 5 minutes, gradual gradient from 10% B to 36% B for 70 minutes, then a step gradient to 100% for 10 minutes, ending with a 5 minute flat elution at 100% B. The total run time was 90 minutes with data collected during the entire duration. The mass spectrometer was operated in data dependent mode with a survey scan ranging from 350-1500 m/z with 60% RF Lens, AGC target of 1E6 charges, and 100 ms maximum injection time. Peptides of charge state 2+ to 6+ were included. Dynamic exclusion range was set to 60 seconds with mass tolerance of 10 ppm. Selected peptides were fragmented using 30% HCD collision energy, and the resultant MS2 spectrum was acquired using the Orbitrap with a resolution of 15k and AGC target of 5E4 charges with maximum injection time of 22 ms.

QUANTIFICATION AND STATISTICAL ANALYSIS

Cell cycle analysis

The nuclear cycle (NC) time for embryos expressing CycE-sfGFP was analyzed similarly to the method describe by Chari et al.[57] In brief, the duration of an NC was calculated from the number of frames between the appearance of CycE-sfGFP in at least 50% of the nuclei in the embryo and the re-appearance of CycE-sfGFP in at least 50% of the nuclei in the next NC.

Quantitative phosphoproteomic data processing

The Gygi Lab GFY software licensed from Harvard was used to convert RAW file to the mzXML format, and to correct erroneous assignments of peptide ion charge state and monoisotopic m/z. MS2 spectra were assigned using the SEQUEST algorithm. Data was searched against the D. melanogaster proteome reference dataset acquired from UniProt (Proteome ID UP000000803, Protein count 21973) with forward and reversed sequences concatenated as per the target-decoy strategy. SEQUEST searches were performed using a 20 ppm precursor ion tolerance where both N and C-termini were required to be consistent with the protease specificity of Lys-C and Trypsin. Fragment ion tolerance in the MS3 spectrum was set at 1 Th. N-ethylmaleimide (+125.047679 Da) was set as a static modification on cysteine residues. TMTpro tags (+304.2071 Da) were set as static modifications on lysine residues and N termini. Oxidation of methionine (+15.99492 Da) and phosphorylation of serine, tyrosine, and threonine (+79.9663304104 Da) were set as variable modifications. A peptide-level MS2 spectral assignment false discovery rate (FDR) of 1% was applied as previously described by Johnson et al.[56] The linear discriminant analysis used the following features: SEQUEST parameters XCorr and ΔXCorr, charge state, peptide length and absolute peptide mass accuracy.

Phosphopeptides with isolation specificity greater than 0.5 and sum of raw TMTpro signal-to-noise (S/N) ion intensities greater than 200 for 10 min optoSos or 100 for 3 min optoSos were included for further analysis. The raw S/N ion intensities were normalized as follows: (1) each TMTpro ion intensity for a given phosphopeptide was divided by the average TMTpro ion intensity observed in all acquired TMTpro channels for that phosphopeptide, and (2) for each channel, values from step 1 were normalized by the median step 1 value of all flowthrough (non-phosphorylated) peptides in the corresponding channel. The TMTpro intensity fold-change for a given phosphopeptide between the light and no light conditions were calculated by dividing the average normalized intensity for the "light" channels by that for the "no light" channels. Student's t-test was used to assign statistical significance for changes in phosphopeptide abundance. P-values were adjusted by the Benjamini-Hochberg procedure.[58,59] For the analysis of localized phosphorylation sites, only sites with max Ascore/ModScore >= 13 were considered.[60,61]

Inferring kinase activity

Scoring and matching

We explore two strategies for evaluating kinase activity: an approach comparing substrates within the experiment and another comparing against a hypothetical fly phosphoproteome. Both require predicting the kinase(s) which match/phosphorylate each of the discovered substrates using the procedure described by Johnson et al.[30] In brief, the sequences of the phosphopeptides are scored using the position-specific scoring matrices (PSSM) of the kinases in Johnson et al.[30] For each kinase, its scores are ranked against a background of scores from a putative set of phosphopeptides,[62] and a score is considered a match if it is in the top 10 percentile of background scores, as suggested by Johnson et al.[30] We provide a schematic in Figure S3. To reduce the number of spurious matches, we restrict our analysis to the set of human kinases that have a fly ortholog, are not membrane-bound, and are expressed during nuclear cycle 14. Fly and human kinases were considered orthologs if they were found to be reciprocal best hits using BLAST. This reduces the number of considered kinases from the 303 found in Johnson et al.[30] to 56.

z-test statistic on kinase activity

The first approach to determine kinase activity uses a one sample z-test.[63] For each of the 56 kinases, we compare the mean of the $\log_2$ fold-change (FC) in phosphorylation of matches to the kinase against the $\log_2$FC distribution of all detected peptides. For each kinase, we compute the one-sided z-test statistic, $\frac{x-\mu_0}{\sigma/\sqrt{n}}$, where x is the average $\log_2$FC of the peptides that match the kinase, n is number of peptides that match that kinase, and μ_0 and σ are the average $\log_2$FC and standard deviation, respectively, of all detected peptides. If $x > \mu_0$, the z-test is converted to a one-tailed p-value using a standard normal distribution and computing the probability that $\mu_0 \geq x$, and otherwise the p-value is computed as that $\mu_0 \leq x$. Finally, the p-values are adjusted for a false discovery rate (FDR) of 10% using the Benjamini-Hochberg procedure.[58,59]

Kinase match enrichment

We also use a second approach to uncover the kinases relevant for the experiment. An "enrichment score" is calculated for each kinase, and defined as the fraction of matches to the kinase in the experiment divided by the fraction of matches in the hypothetical fly phosphoproteome. The hypothetical fly phosphoproteome consists of all 10-mers in the proteome expressed in nuclear cycle 14 *Drosophila* embryos (obtained from label-free proteomics described above) where the middle (i.e., sixth) position is either S or T, and each 10-mer is scored and considered as a match for a kinase using the Johnson et al. method.[30] A kinase with a large proportion of matches in the experiment but a relatively low proportion of matches in the phosphoproteome suggests that it has enriched activity in this point in embryogenesis. *P*-values are computed using the hypergeometric distribution, adjusted via the Benjamini-Hochberg procedure.[58,59]